JOURNAL OF GUIDANCE, CONTROL, AND DYNAMICS
Vol. 30, No. 5, September–October 2007

Engineering Notes

ENGINEERING NOTES are short manuscripts describing new developments or important results of a preliminary nature. These Notes should not exceed 2500 words (where a figure or table counts as 200 words). Following informal review by the Editors, they may be published within a few months of the date of receipt. Style requirements are the same as for regular contributions (see inside back cover).

Control and Simulation of Relative Motion for Aerial Refueling in Racetrack Maneuvers

Atilla Dogan* and Eunyoung Kim†
University of Texas at Arlington, Arlington, Texas 76019
and
William Blake‡
U.S. Air Force Research Laboratory, Wright–Patterson Air Force Base, Ohio 45433

DOI: 10.2514/1.29487

I. Introduction

THIS paper focuses on the development of an integrated simulation environment and control algorithms for a receiver aircraft in boom–receptacle refueling (BRR) operation while the tanker flies in a racetrack maneuver. A racetrack maneuver is the standard pattern flown by tanker aircraft, with straight legs and bank turns [1]. This paper applies the earlier work by the authors on mathematical modeling of relative motion [2,3] and aerodynamic coupling [4] to the simulation of aerial refueling, and it develops control laws for the motion of the receiver relative to the tanker that flies in racetrack maneuvers. An integrated simulation environment is developed to take into account tanker maneuvers, motion of the receiver relative to the tanker, and the aerodynamic coupling due to the trailing wake vortex of the tanker. The separate dynamic model of the tanker, including its own controller, allows the simulation of the standard racetrack maneuvers of the tanker in aerial refueling operations. The mathematical model of the receiver expressed in terms of the relative position and orientation with respect to the tanker's body frame facilitates the formulation, in a single framework, of maneuver and stationkeeping of the receiver behind the tanker. For the racetrack maneuvers of the tanker, a linear quadratic regulator (LQR)-based multi-input/multi-output (MIMO) state feedback and integral control technique is developed to track commanded speed, altitude, and yaw rate. Similarly, for the relative motion of the receiver, an LQR-based MIMO state feedback and integral control technique is designed to track the commanded trajectory expressed in the body frame of the tanker. Both controllers schedule their corresponding feedback and integral gains based on the commanded speed and yaw rate of the tanker. The tanker aircraft model represents KC-135R, and the receiver aircraft model is a tailless fighter aircraft with innovative control effectors (ICE) and thrust-vectoring capability. Because the receiver has redundant control variables, various control allocation schemes are investigated for trajectory tracking and stationkeeping while the tanker flies in various racetrack maneuvers with different commanded turn rates.

Presented as Paper 6710 at the AIAA Guidance, Navigation, and Control Conference and Exhibit, Keystone, CO, 21–24 August 2006; received 26 December 2006; revision received 6 June 2007; accepted for publication 7 June 2007.

*Assistant Professor, Department of Mechanical Aerospace Engineering. Senior Member AIAA.
†Graduate Student, Department of Mechanical Aerospace Engineering.
‡Aerospace Engineer. Associate Fellow AIAA.

II. Tanker Dynamics Relative to the Inertial Frame

The performance of an aerial refueling operation depends on the motion of the tanker as much as the motion of the receiver. Thus, for the evaluation of aerial refueling controllers, the simulation environments should include the full dynamic model of the tanker. Further, for a true representation of the aerodynamic coupling due to the trailing wake vortex, the motion of the tanker should be modeled accurately. The motion of the tanker is represented by a standard set of equations that are presented herein to introduce the notation later used for the equations of motion for the receiver. Further, because they are available in the same document, one can easily compare the equations for the tanker with those for the receiver. In this paper, I frame, B_T frame, and W_T frame denote the inertial frame, the body frame of the tanker, and the wind frame of the tanker, respectively.

In matrix form, the translational kinematic equation of the tanker is

$$\dot{r}_{B_T} = \mathbf{R}^{\mathbf{T}}_{\mathbf{B_T I}} \mathbf{R}_{\mathbf{B_T W_T}} V_{w_T} \tag{1}$$

where r_{B_T} is the position of the tanker relative to the I frame expressed in the I frame, $\mathbf{R}_{\mathbf{B_T I}}$ is the rotation matrix from the I frame to the B_T frame, $\mathbf{R}_{\mathbf{B_T W_T}}$ is the rotation matrix from the W_T frame to the B_T frame, and V_{w_T} is the velocity of the tanker relative to the local air expressed in the W_T frame.

The translational dynamic equation of the tanker aircraft in matrix form is

$$\begin{bmatrix} \dot{V}_T \\ \dot{\beta}_T \\ \dot{\alpha}_T \end{bmatrix} = \mathcal{E}^{-1}_{\mathbf{T}} \mathbf{S}(\omega_{\mathbf{B_T}}) \mathbf{R}_{\mathbf{B_T W_T}} V_{w_T} + \frac{1}{m_T} \mathcal{E}^{-1}_{\mathbf{T}} (\mathbf{R}_{\mathbf{B_R I}} M_T \mathbf{R}_{\mathbf{B_T W_T}} A_T + P_T) \tag{2}$$

where $\mathcal{E}_{\mathbf{T}}$ is a 3×3 matrix that depends on α_T, β_T, and V_T [5]. The external forces acting on the tanker are the gravitational force $M_T = [0 \;\; 0 \;\; m_T g]^T$ (in the I frame), the aerodynamic force $A_T = [-D_T \;\; -S_T \;\; -L_T]^T$ (in the W_T frame), and propulsive force $P_T = [T_T \cos\delta_T \;\; 0 \;\; -T_T \sin\delta_T]^T$ (in the B_T frame). Note that g is the gravitational acceleration; m_T is the mass of the tanker; D_T, S_T, and L_T are the drag, side force, and lift on the tanker, respectively; T_T is the thrust magnitude; and δ_T is the thrust inclination angle. Also note that $\mathbf{S}(\cdot)$ is the skew-symmetric matrix operation on the representation of a vector [5]. The details of the aerodynamic coefficients in the standard expressions for the aerodynamic forces can be seen in [5].

The rotational kinematic equation in matrix form is the standard equation:

$$\mathbf{R}_{\mathbf{B_T I}} \dot{\mathbf{R}}_{\mathbf{B_T I}} = -\mathbf{S}(\omega_{\mathbf{B_T}}) \tag{3}$$

where $\omega_{\mathbf{B_T}} = [p_T \;\; q_T \;\; r_T]^T$ is the representation of the angular

velocity vector of the tanker relative to the I frame expressed in the B_T frame. In the simulation and control design, standard rotational kinematic equations (in terms of the Euler angles ψ_T, θ_T, and ϕ_T) are used.

The matrix form of the rotational dynamic equation of the tanker is

$$\dot{\omega}_{B_T} = \underline{\mathbf{I}}_{\mathbf{T}}^{-1} M_{B_T} + \underline{\mathbf{I}}_{\mathbf{T}}^{-1} \mathbf{S}(\omega_{\mathbf{B_T}}) \underline{\mathbf{I}}_{\mathbf{T}} \omega_{B_T} \tag{4}$$

where $\underline{\mathbf{I}}_{\mathbf{T}}$ is the inertia matrix of the tanker aircraft, and $M_{B_T} = [\mathcal{L}_T \;\; \mathcal{M}_T \;\; \mathcal{N}_T]^T$ is the moment of the external forces about the origin of the B_T frame and expressed in the B_T frame. For the components of the applied moments, standard expressions are used, with the exception that the pitching moment has contribution from the thrust with the moment arm Δ_{z_T}. The details of the aerodynamic moment coefficients are given in [5].

Note that the stability derivatives are considered to be constant for the flight conditions studied in this paper. The dynamics of the engine is modeled as a first-order transfer function in terms of throttle setting ξ_T, with a constant maximum thrust $T_{\max_T}$. For the control surfaces, actuator saturation is taken into account, with -20 to 20 deg limits.

III. Receiver Dynamics Relative to the Tanker

In an efficient aerial refueling operation, the receiver aircraft needs to be controlled with respect to the tanker's position and orientation, rather than with respect to the inertial reference. A new set of nonlinear equations derived earlier [2] is used herein to represent the position and orientation of the receiver relative to the tanker and, at the same time, to explicitly represent the vortex effect on the dynamics of the receiver aircraft. The matrix form of the equations are given next, because they are used in the simulation of the closed-loop system. In this paper, B_R frame and W_R frame denote the body frame and wind frame of the receiver, respectively.

The translational kinematic equation is written [2] in terms of the position vector of the receiver with respect to the tanker:

$$\dot{\xi} = \mathbf{R}^{\mathbf{T}}_{\mathbf{B_R B_T}} \mathbf{R}_{\mathbf{B_R W_R}} V_w + \mathbf{R}^{\mathbf{T}}_{\mathbf{B_R B_T}} W - \mathbf{R}_{\mathbf{B_T I}} \dot{r}_{B_T} + \mathbf{S}(\omega_{\mathbf{B_T}}) \xi \tag{5}$$

where $\xi = [x \;\; y \;\; z]^T$ is the position of the receiver relative to the tanker expressed in the B_T frame, $\mathbf{R}_{\mathbf{B_R W_R}}$ is the rotation matrix from the W_R frame to the B_R frame, V_w is the velocity of the receiver relative to the local air expressed in the W_R frame, W is the velocity of the local air relative to the ground expressed in the B_R frame, $\mathbf{R}_{\mathbf{B_R B_T}}$ is the rotation matrix from the B_T frame to the B_R frame, $\mathbf{R}_{\mathbf{B_T I}}$ is the rotation matrix from the I frame to the B_T frame, and $\dot{r}_{B_T}$ is the velocity of the tanker relative to the I frame.

The translational dynamic equation of the receiver, including the wind effect, is [2]

$$\begin{bmatrix} \dot{V} \\ \dot{\beta} \\ \dot{\alpha} \end{bmatrix} = \mathcal{E}^{-1}_{\mathbf{R}} [\mathbf{S}(\omega_{\mathbf{B_R B_T}}) + \mathbf{R}_{\mathbf{B_R B_T}} \mathbf{S}(\omega_{\mathbf{B_T}}) \mathbf{R}^{\mathbf{T}}_{\mathbf{B_R B_T}}] (\mathbf{R}_{\mathbf{B_R W_R}} V_w + W)$$
$$- \mathcal{E}^{-1}_{\mathbf{R}} \dot{W} + \frac{1}{m} \mathcal{E}^{-1}_{\mathbf{R}} (\mathbf{R}_{\mathbf{B_R B_T}} \mathbf{R}_{\mathbf{B_T I}} M_R + \mathbf{R}_{\mathbf{B_R W_R}} A_R + P_R) \tag{6}$$

where $\mathcal{E}^{-1}_{\mathbf{R}}$ is of the same form as $\mathcal{E}^{-1}_{\mathbf{T}}$, with V, β, and α replacing V_T, β_T, and α_T, respectively. M_R and A_R are the representations of the gravitational and aerodynamic force vectors, respectively, and are defined similar to the corresponding vectors of the tanker. Because of the fact that the receiver aircraft has thrust-vectoring capability, $P_R = [T_x \;\; T_y \;\; T_z]^T$ has three components in the B_R frame as functions of δ_y and δ_z, the angles of the thrust vector with the x–y and x–z planes of the B_R frame, respectively. The details of thrust-vectoring formulation and the aerodynamic coefficients in the standard expressions for the aerodynamic forces are given in [5].

The rotational motion of the receiver aircraft, similar to its translational motion, is also analyzed with reference to the B_T frame, which is an accelerating and rotating reference frame:

$$\mathbf{R}_{\mathbf{B_R B_T}} \dot{\mathbf{R}}^{\mathbf{T}}_{\mathbf{B_R B_T}} = -\mathbf{S}(\omega_{\mathbf{B_R B_T}}) \tag{7}$$

where $\omega_{\mathbf{B_R B_T}} = [p \;\; q \;\; r]^T$ is the representation in the B_R frame of the angular velocity vector of the receiver aircraft relative to the B_T frame. Similar to the tanker's case, simulations and control design use the standard rotational kinematic equations (in terms of Euler angles ψ, θ, and ϕ).

The rotational dynamics of the receiver are modeled as

$$\dot{\omega}_{B_R B_T} = \underline{\mathbf{I}}_{\mathbf{R}}^{-1} M_{B_R} + \underline{\mathbf{I}}_{\mathbf{R}}^{-1} \mathbf{S}(\omega_{\mathbf{B_R B_T}} + \mathbf{R}_{\mathbf{B_R B_T}} \omega_{\mathbf{B_T}})$$
$$\underline{\mathbf{I}}_{\mathbf{R}} (\omega_{B_R B_T} + \mathbf{R}_{\mathbf{B_R B_T}} \omega_{B_T}) - \mathbf{S}(\omega_{\mathbf{B_R B_T}}) \mathbf{R}_{\mathbf{B_R B_T}} \omega_{B_T} - \mathbf{R}_{\mathbf{B_R B_T}} \dot{\omega}_{B_T} \tag{8}$$

where $\underline{\mathbf{I}}_{\mathbf{R}}$ is the inertia matrix of the receiver aircraft, and $M_{B_R} = [\mathcal{L} \;\; \mathcal{M} \;\; \mathcal{N}]^T$ is the moment due to aerodynamics and thrust vectoring about the origin of the B_R frame and expressed in the B_R frame.

As in the case of the tanker, the stability derivatives of the receiver are constant. Further, the engine model of the receiver is also a first-order transfer function with constant maximum thrust. For the actuator dynamics, actuator saturation and rate limit effects are considered for the receiver. The deflection range attainable from the elevon is -30 to 30 deg, from the pitch flap is -30 to 30 deg, and from the clamshell is -60 to 60 deg. All three control effectors have a rate limit of ± 90 deg/s. Likewise, the thrust vectoring has a limit of ± 30 deg in both directions and a rate limit of ± 30 deg/s.

Note that the motions of the tanker aircraft, both translational and rotational, are represented as exogenous inputs in the equations of motion of the receiver aircraft.

IV. Modeling the Effect of the Trailing Vortex

It is to be noted that the wind effect terms W and $\dot{W}$ in the receiver's equations of motion presented earlier are based on the uniform wind distribution acting at the receiver's center of mass expressed in the B_R frame. However, the vortex-induced wind field acting on the receiver aircraft is nonuniform in nature. For the dynamic modeling of the vortex effect in aerial refueling, the tanker is considered to produce two pairs of straight, semi-infinite, trailing vortex filaments (one from the wings and one from the horizontal tail) that induce additional wind velocities on the body of the receiver aircraft. The induced wind is written as a function of the relative separation and of the relative orientation between the tanker and the receiver using a modified horseshoe-vortex model based on the Helmholtz profile. Because the induced wind and wind gradients are nonuniform along the body dimensions of the receiver aircraft, an averaging technique is employed to compute the effective wind and wind gradient as uniform approximations. The effective wind components and gradients are introduced into the nonlinear aircraft equations that include the components of wind and the temporal variation of wind in the B_R frame. The effect of vortex decay over time is also included in our model. Special care was taken to accommodate different geometrical dimensions for the tanker and receiver aircraft. Many geometrical parameters considered include the wing's sweep angle and dihedral angle and the relative distance between the center of mass of the aircraft and the aerodynamic center of the wing. Previous publications [2–4] of the authors should be referred to for further details of the actual vortex model and the averaging technique used to estimate the vortex effect on the receiver.

V. Control Design

For a successful aerial refueling operation, the receiver should approach the tanker, stay at the refueling contact position during the actual fuel transfer, and fly away once the refueling is completed, all in a safe manner, despite various sources of disturbance such as trailing wake vortex, fuel transfer, and motion of the tanker. A reference trajectory for the motion of the receiver relative to the tanker should include 1) the approach from the observation position to the contact position, 2) stationkeeping at the contact position, and 3) the fly-away. These three phases of aerial refueling can easily be addressed in a single framework by using the equations of motion of receiver, derived relative to the tanker. Obviously, during the phase in which the receiver should stay at the refueling contact position

(stationkeeping phase), the reference trajectory for the receiver becomes a point in the B_T frame.

The primary requirement of the control design is the tracking of the reference trajectory, with zero steady-state error in the x, y, and z coordinates in the B_T frame, under the disturbance of trailing vortex, time variation of the inertia properties of the receiver, and the possible steady maneuvers of the tanker. Furthermore, the control inputs generated by the controller should not cause significant saturation on the magnitudes and rates of the actuators. During a transient phase, overshoot or undershoot on trajectory response should be minimized to ensure the safety of the refueling. At the same time, the response of the closed-loop system should be fast enough so that the approach and fly-away maneuvers are completed as planned and the high-wind regions of the trailing vortex field are exited in a timely fashion. Additionally, the angle of attack and the airspeed should not be close to their corresponding stall values. In this regard, a very large pitch angle should not be commanded. Finally, to ensure the safety of the aircraft, the bank angle should be small relative to its nominal value. As stated earlier, the controller should perform satisfactorily in all legs of the racetrack maneuver.

To satisfy all of the requirements, a combination of a multi-input/multi-output state-feedback LQR and integral control technique is employed in designing the position-tracking controller for the six control variables, three control surfaces, two thrust-vectoring angles, and throttle. Moreover, a gain-scheduling scheme is implemented based on the speed and turn rate. The equations of motion given in Sec. III are linearized at four different steady-state-trimmed nominal conditions. In the linearization, the wind terms are ignored. Two of the nominal conditions correspond to the tanker flying at a straight level (i.e., $\dot{\psi}_{T,1} = 0$) at constant altitude with two different airspeeds ($V_{T,1}$ and $V_{T,2}$), and the other two correspond to the tanker turning with a specified turn rate of $\dot{\psi}_{T,2}$ at a constant altitude with the same two airspeeds.

Note that the control law assumes the availability of full state measurement or estimation for feedback. Further, for the implementation of the gain-scheduling scheme, the commanded speed and yaw rate of the tanker should be communicated to the receiver.

Note also that the controller used for the tanker aircraft in the simulations is designed similarly for the three conventional control surfaces and the throttle setting. The outputs to be controlled are the airspeed, altitude, and yaw rate. Gain scheduling is based on the commanded speed and the yaw rate, and the four nominal conditions defined earlier are used for the design of the linear controllers. The details of the controller designs can be found in [5].

VI. Simulation Results

The four nominal conditions used in the gain-scheduling controller are 1) $\dot{\psi}_T = 0$ and $V_T = 180$ m/s, 2) $\dot{\psi}_T = 0$ and $V_T = 200$ m/s, 3) $\dot{\psi}_T = 1.7$ deg/s and $V_T = 180$ m/s, and 4) $\dot{\psi}_T = 1.7$ deg/s and $V_T = 200$ m/s. The LQR/integral controllers are designed and implemented in such a way that various levels of control input allocations can be tested. Three different control allocation cases are designed by choosing the weighting matrices of the LQR cost function accordingly (for numerical values, see [5]). Case 1 is when a combination of control effectors and thrust vectoring is used. In case 2, only control effectors are used, without any thrust vectoring. In case 3, the pitch flap and clamshell are fixed at their nominal values; elevon and thrust vectoring are the only control variables used.

The full six-DOF nonlinear dynamics of both tanker and receiver, along with the controllers designed, are simulated in an integrated environment, including the trailing wake vortex. The refueling is performed at the nominal altitude of 7010 m, and the tanker is flying at the speed of 200 m/s. The tanker is initially in a straight-level flight and stays in this condition until the receiver aircraft moves from the observation position to the refueling contact position. Then the tanker starts turning until a U-turn is completed, and the receiver is commanded to stay at the contact position.

Three cases of tanker turn with different turning rates are simulated. The commanded yaw rate for tanker case 1 is generated from a 1.7-deg/s step response of a fourth-order linear filter with time constants of 10, 10, 10, and 1 s. Tanker case 2 is a 2.2-deg/s step response of the same filter. Tanker case 3 is a 1.7-deg/s step response of a second-order linear filter with two time constants of 10 s. Recall that the tanker model has its own gain-scheduling controller to track the commanded altitude, speed, and yaw rate. For the receiver's gain-scheduling controller, the same step signals for the yaw rate, after passing through a first-order filter with a time constant of 10 s, are used for scheduling purposes. The first plot of Fig. 1 shows the x–y projections of the entire target trajectories. The second plot shows the altitude histories only during the turn. Note that the tanker altitude slightly deviates from the nominal altitude during the turns, which, although small for the tanker, is very significant for the performance of the refueling. Figure 2 shows the pitch and bank angles of the tanker, which directly change the relative orientation and thus cause the refueling position to move. Although not shown here, airspeed, angle of attack, and sideslip angle of the tanker also vary during the turns, which affects the wind field in the wake of the tanker.

Figure 3 illustrates the x, y, and z components of the trajectory of the receiver in the B_T frame in case 1 (the other cases yield similar results). The receiver is initially at the observation position (−40.56, 60.96, and 6.46) in the B_T frame and should move to the refueling contact position (−25.33, 0, and 6.46) without any altitude change. The lateral maneuver is initiated at around 50 s and takes about a minute until the receiver is directly behind the tanker. Then at 125 s, the receiver starts moving forward and reaches the refueling contact position in about 50 s. The figure shows that the commanded trajectories are closely tracked during the maneuver. The two spikes in the z plot are due to slight altitude loss (the positive z direction is down) that occurs when the lateral and forward maneuvers start.

Figures 4–6 show the time history of the control variables in all three control allocation cases and in tanker case 1 (the other tanker-

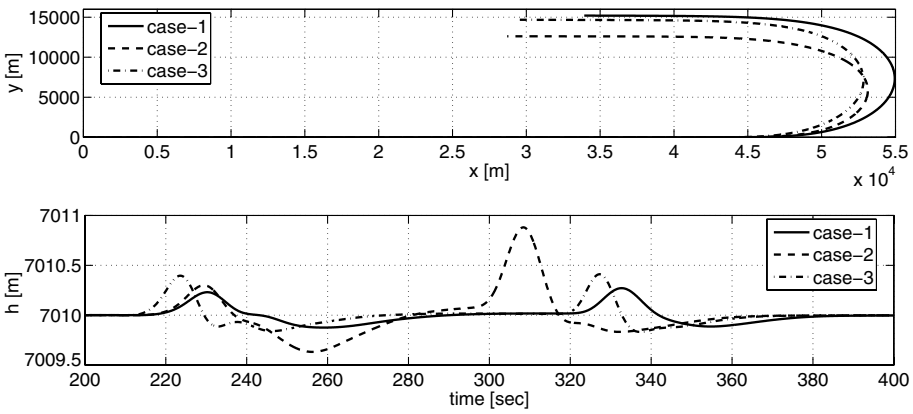

Fig. 1 Target trajectories and altitude histories during turns with three different yaw rates.

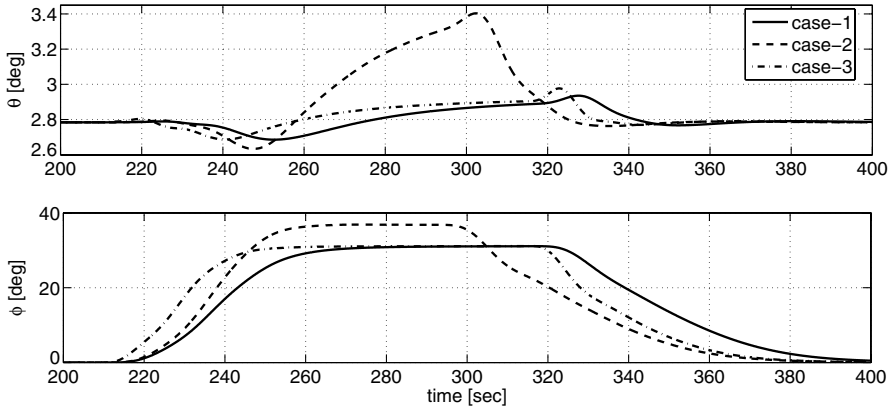

Fig. 2 Pitch and bank angles of tanker during the turns.

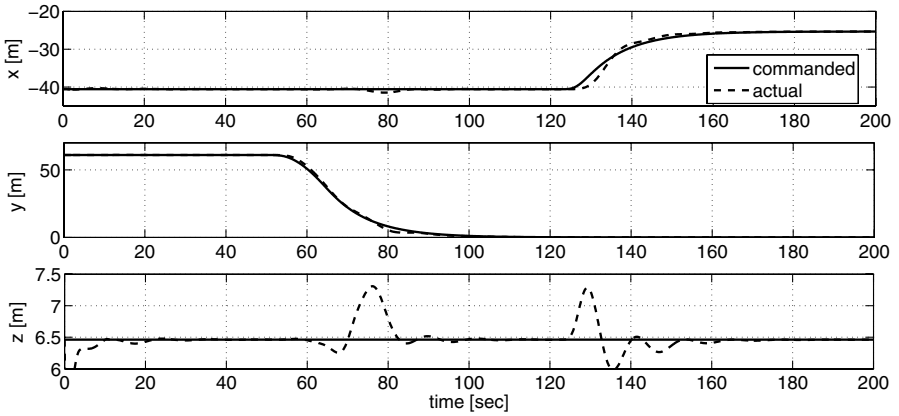

Fig. 3 Commanded and actual x, y, and z positions of the receiver during the approach maneuver.

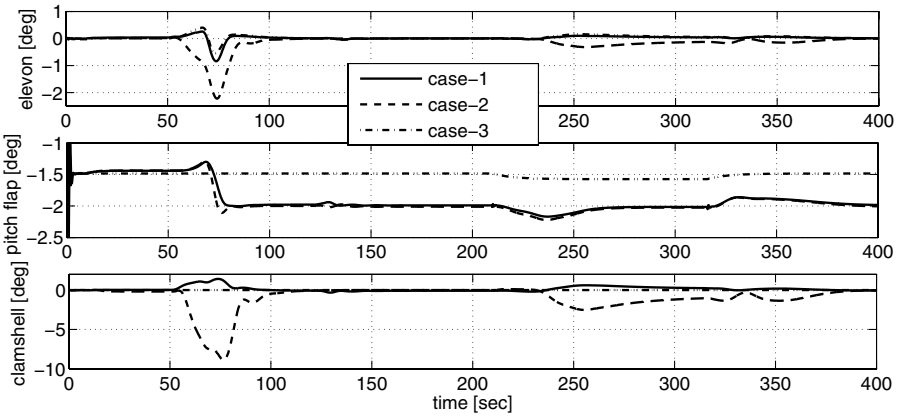

Fig. 4 Deflection of the three control effectors in the three cases.

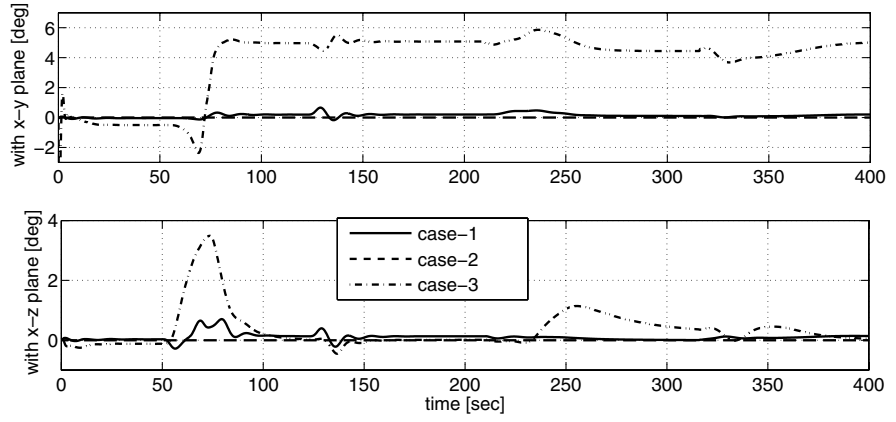

Fig. 5 Thrust-vectoring angle variation in the three cases.

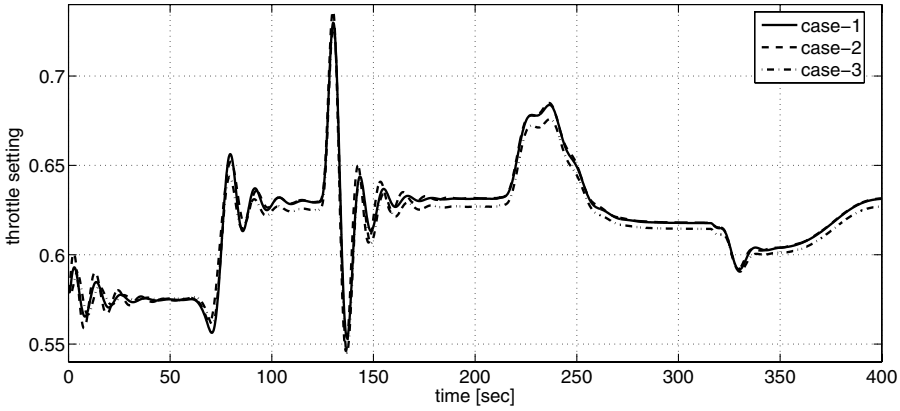

Fig. 6 Variation in throttle level in the three cases.

turn cases yield similar results). Figure 4 illustrates the deflections of the three control effectors. Note that the pitch flap and clamshell stay almost constant in case 3, because they are fixed at their nominal values. In all cases, very small deflections and deflection rates (much smaller than their respective saturation levels) in all three effectors are used to move the receiver to the refueling position and keep it there during the turns. Both the elevon and clamshell are mainly used during the lateral maneuver. Although the control effectors are used during the turn, their deflections are smaller than the deflections in the time of the approach maneuver. Figure 5 shows the rotation of the thrust vector in terms of its angles with the x–y and x–z planes of the B_R frame. Note that both angles stay zero in case 2, because it represents a no-thrust-vectoring configuration. Thrust vectoring is used mostly in case 3, in which the pitch flap and clamshell are fixed. The rotation of the thrust vector is small in case 1, because it is used in combination with the control surfaces.

Figure 6 illustrates the level of throttle in the three cases. In all cases, the variation of throttle setting is very similar. Note the increase in the throttle setting (60–100 s) during the lateral maneuver. This is because when the receiver aircraft is behind the tanker, it is subject to strong downwash, which results in higher required thrust. The slight difference in throttle between the cases near 200 s is due to the different thrust-vectoring angles and different orientation of the aircraft at the refueling position. Variations of throttle setting in the three tanker-turn cases during the turn of the tanker (after 200 s) are similar, and the levels of throttle setting before and after the turn are the same.

Figure 7 shows that the orientation of the receiver relative to the tanker changes during the approach maneuvers and the tanker turn in the three cases. Note that during both the approach maneuver and the tanker turn, the orientation of the receiver is close to the orientation of the tanker. Comparison of the yaw response in case 2 (no thrust vectoring) with the other two cases in which thrust vectoring is used indicates the positive effect of thrust vectoring in yaw motion during both lateral maneuver and tanker turn.

The vortex-induced wind components and gradients are shown in Fig. 8 in the control allocation case 1 and tanker case 1. When the simulation starts, the vortex is not on and at 10 s, the wind is turned on and gradually increased to the normal level. First note that once the vortex is turned on at 10 s, the aircraft is exposed to small upwash and side wash and a slight "rolling" gradient. During the lateral maneuver (starting at 50 s), the magnitudes of both effective wind components and gradients increase. At about 70 s when the lateral distance to the tanker is about 60% of the tanker's wingspan, the highest upwash (negative W_z) is experienced. When the lateral distance to the tanker is about 45% of the tanker's wingspan, the receiver experiences the greatest rolling vortex P and the upwash turns into downwash (positive W_z), whereas the side wash W_y increases dramatically. This is manifested in the rolling oscillation in Fig. 7 and the altitude drop in Fig. 3. During this transition, a yawing vortex R gradient is experienced and a pitching vortex Q gradient develops. As the receiver moves right behind the tanker, the rolling vortex gradient and side wash disappear and downwash increases to its highest level. When the receiver is right behind the tanker, two main vortex effects remain: strong downwash and pitching vortex. Note the small variation in the wind components and gradients during the tanker turn. This is partly because the receiver relative position and orientation experience small deviation and partly because the tanker's airspeed, angle of attack, and sideslip angle change when the tanker turns.

To maintain the refueling contact while the target turns, the position and orientation deviations should remain small. To analyze the performance of the controllers in terms of these important requirements, phase portraits of position and orientation, based on the data during the tanker turns, are presented in Figs. 9 and 10 in tanker case 2. Note that the y deviation stays within 1.3 and −0.9 m and the x deviation is between −0.8 and 0.9 m in all three control allocation cases. Regarding the z deviation, case 3 is worse than the others. This is apparently due to the fact that the pitch flap is stuck and thrust vectoring is used instead to generate pitching moment. In all

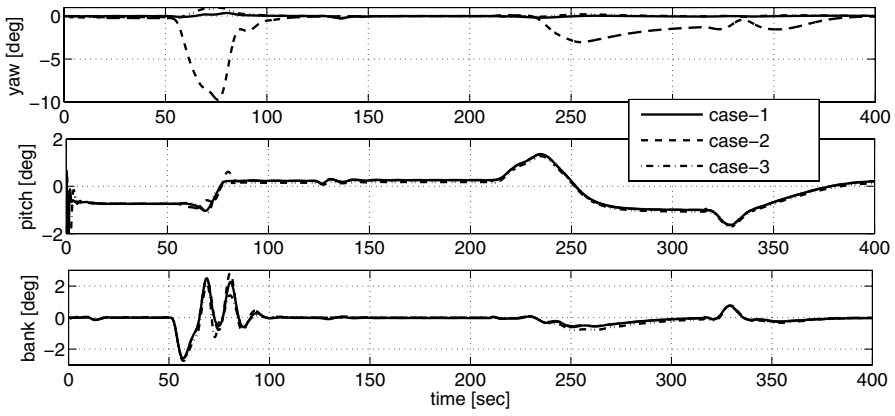

Fig. 7 Orientation of the aircraft relative to the tanker in the three cases.

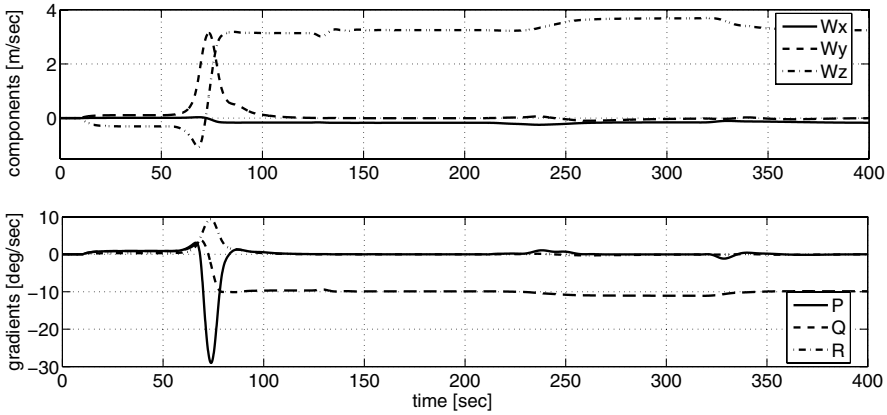

Fig. 8 Wind components and gradients to which the receiver is exposed in case 1.

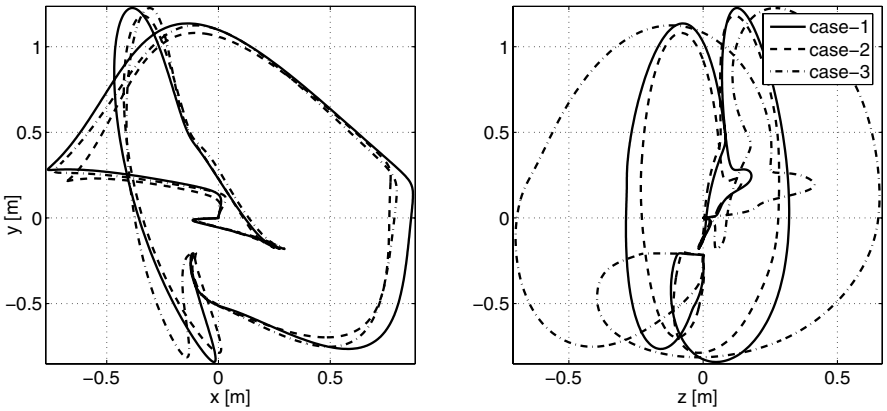

Fig. 9 Deviation of the receiver position from the refueling position when the tanker turns in tanker case 2.

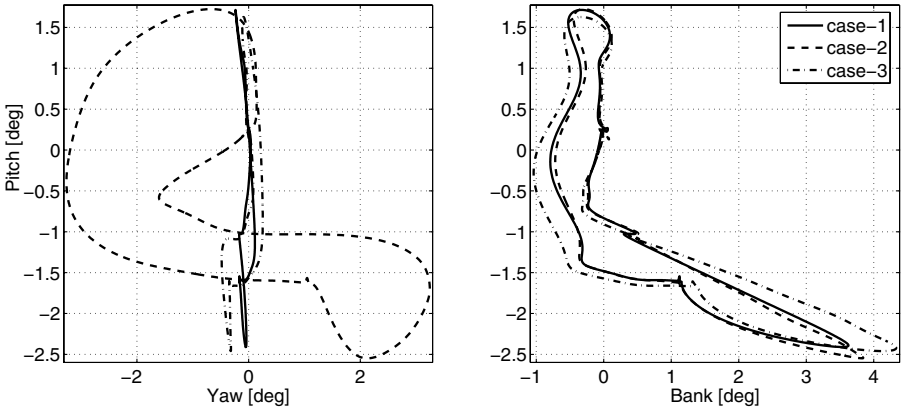

Fig. 10 Deviation in relative orientation when the tanker turns in tanker case 2.

three cases, the receiver stays close to the tanker, in terms of orientation. Pitch-angle variation is about the same for all cases, whereas case 2 shows larger deviation in yaw, and case 3 yields slightly larger deviation in bank. As shown in Fig. 1, tanker case 2 has the sharpest turn with the largest bank. As a result, the receiver aircraft experiences the largest deviations in this case, in comparison with the other two tanker-turn cases, which are not presented in this paper. For example, in tanker case 1, the position deviations are limited to −0.6 to 0.8 m in the y direction and −0.6 to 0.5 m in the x direction, whereas the three control allocation cases show a similar trend when compared with each other.

VII. Conclusions

The maneuvering tanker influences the relative motion via two mechanisms:

1) The tanker motion acts as a direct disturbance on the relative motion; for example, when the tanker banks, the contact position moves laterally.

2) The maneuvers of the tanker change the trailing vortex field to which the receiver aircraft is exposed.

Simulation results also show that by adjusting the weighting matrices, the LQR method can easily provide an effective control allocation between the control effectors and thrust vectoring. Simulation results show that all three control allocation schemes can effectively follow the commanded trajectory without excessive control effort through the wind field, even if the controller design is based on the linearized equations without the wind terms. When the receiver moves in the wake of the tanker, the simulation shows that the induced wind components and the gradients vary. Phase-portrait plots demonstrate that the stationkeeping performance during the tanker turn is affected mostly by the rate of turn. The linearization of

the equations of motion results in a clear manifestation of the tanker motion as disturbance on the relative motion. This formulation has the potential of improving the stationkeeping performance during the tanker turns and will be the subject of our future work.

References

[1] Nalepka, J. P., and Hinchman, J. L., "Automated Aerial Refueling: Extending the Effectiveness of Unmanned Air Vehicles," AIAA Modeling and Simulation Technologies Conference and Exhibit, San Francisco, CA, AIAA Paper 2005-6005, 2005.

[2] Venkataramanan, S., and Dogan, A., "Dynamic Effects of Trailing Vortex with Turbulence and Time-Varying Inertia in Aerial Refueling," AIAA Atmospheric Flight Mechanics Conference and Exhibit, Providence, RI, AIAA Paper 2004-4945, Aug. 2004.

[3] Dogan, A., and Venkataramanan, S., "Nonlinear Control for Reconfiguration of Unmanned-Aerial-Vehicle Formation," *Journal of Guidance, Control, and Dynamics*, Vol. 28, No. 4, July–Aug. 2005, pp. 667–678.

[4] Dogan, A., Venkataramanan, S., and Blake, W., "Modeling of Aerodynamic Coupling Between Aircraft in Close Proximity," *Journal of Aircraft*, Vol. 42, No. 4, July–Aug. 2005, pp. 941–955.

[5] Kim, E., "Control and Simulation of Relative Motion for Aerial Refueling in Racetrack Maneuver," M.S. Thesis, Univ. of Texas at Arlington, Arlington, TX, 2007.